Wang and Choi
Micro and Nano Systems Letters (2022) 10:17
https://doi.org/10.1186/s40486-022-00160-9

Micro and Nano Systems Letters

LETTER

Open Access

Highly stretchable strain sensors with improved sensitivity enabled by a hybrid of carbon nanotube and graphene

Leilei Wang and Jungwook Choi*

Abstract

The development of high-performance strain sensors has attracted significant attention in the field of smart wearable devices. However, stretchable strain sensors usually suffer from a trade-off between sensitivity and sensing range. In this study, we investigate a highly sensitive and stretchable piezoresistive strain sensor composed of a hybrid film of 1D multi-walled carbon nanotube (MWCNT) and 2D graphene that forms a percolation network on Ecoflex substrate by spray coating. The mass of spray-coated MWCNT and graphene and their mass ratio are modulated to overcome the trade-off between strain sensitivity and sensing range. We experimentally found that a stable percolation network is formed by 0.18 mg of MWCNTs (coating area of 200 mm^2), with a maximum gauge factor (GF) of 1,935.6 and stretchability of 814.2%. By incorporating the 0.36 mg of graphene into the MWCNT film (i.e., a mass ratio of 1:2 between MWCNT and graphene), the GF is further improved to 12,144.7 in a strain range of 650–700%. This high GF is caused by the easy separation of the graphene network under the applied strain due to its two-dimensional (2D) shape. High stretchability originates from the high aspect ratio of MWCNTs that bridges the randomly distributed graphenes, maintaining a conductive network even under sizeable tensile strain. Furthermore, a small difference in work function between MWCNT and graphene and their stable percolation network enables sensitive UV light detection even under a significant strain of 300% that cannot be achieved by sensors composed of MWCNT- or graphene-only. The hybrids of MWCNT and graphene provide an opportunity to achieve high-performance stretchable devices.

Keywords: Stretchable device, Strain sensor, Carbon nanomaterials, Heterogeneous materials, Sensitivity

Introduction

With the development of wearable devices, the significant potential of strain sensors in healthcare, human–machine interfaces, and soft robotics has led to the desire for high sensitivity, flexibility, and stretchability [1, 2]. Polymer composites consisting of an electrically conductive sensing layer and a polymer matrix have attracted much attention in the field of piezoresistive strain sensors because of their high flexibility and excellent mechanical and electrical properties [3]. One-dimensional (1D) carbon nanotubes (CNTs) [4, 5], metal nanowires [6–8], and two-dimensional (2D) graphene [9, 10] and MXene [11, 12] are widely used as a sensing layer to fabricate strain sensors with high stretchability and sensitivity. In strain sensors, the fracture-prone nature of the contact points between 2D nanomaterials with initial large contact areas contributes to the high sensitivity, while 1D nanomaterials can withstand larger strains without breaking the conductive paths because of their high aspect ratio [13, 14].

Therefore, combining the advantages of 1D and 2D nanomaterials provides an opportunity to produce strain sensors with both high gauge factor (GF) and high stretchability. The GF, a measure of strain sensitivity, is defined as the ratio between relative resistance change and applied strain. Previous studies found that a sensor composed of spray-coated CNTs exhibited

*Correspondence: choij@cau.ac.kr

School of Mechanical Engineering, Chung-Ang University, Seoul 06974, Republic of Korea

Springer Open

© The Author(s) 2022. **Open Access** This article is licensed under a Creative Commons Attribution 4.0 International License, which permits use, sharing, adaptation, distribution and reproduction in any medium or format, as long as you give appropriate credit to the original author(s) and the source, provide a link to the Creative Commons licence, and indicate if changes were made. The images or other third party material in this article are included in the article's Creative Commons licence, unless indicated otherwise in a credit line to the material. If material is not included in the article's Creative Commons licence and your intended use is not permitted by statutory regulation or exceeds the permitted use, you will need to obtain permission directly from the copyright holder. To view a copy of this licence, visit http://creativecommons.org/licenses/by/4.0/.

a sensing range of ~ 90% and a GF of ~ 433.3 in a strain range of ~ 40–70%, while the $Ti_3C_2T_x$-based sensor exhibited improved sensitivity, but its stretchable range was limited to ~ 35% [15]. In contrast, the co-integration of CNTs and $Ti_3C_2T_x$ enables the sensor to achieve a wide stretchable range (~ 75%) and high sensitivity (GF of 772.6 in a strain range of ~ 40–70%) [15]. Furthermore, the strain sensors fabricated by embedding silver nanofibers into flexible substrate exhibit a three-orders-of-magnitude increase in GF after incorporating 2D molybdenum disulfide nanosheets [16].

Among many possible combinations of 1D and 2D nanomaterials for stretchable, sensitive strain sensors, carbon nanomaterials such as CNTs and graphene would be suitable candidates because of their excellent conductivity, stability, flexibility, various morphology, and low toxicity [17, 18]. The 1D CNT-based strain sensors typically have a wide strain range but relatively small GF. The strain sensor fabricated from aligned single-walled CNT films can detect electrical signal changes in the 280% strain range with a maximum GF of only ~ 0.82 [4]. The spray-coated CNTs on Ecoflex have a stretchable range up to 1,380% but low sensitivity (~ 1.75 of GF) [19]. In contrast, the 2D graphene-based strain sensors usually have a large GF in the limited sensing range. The graphene flake-PDMS strain sensor fabricated by the self-assembly technique has a GF as high as 1037 in the 2% stretchable range [20]. Therefore, combining 1D CNT and 2D graphene should result in a wide strain range and high sensitivity in a stretchable strain sensor. In addition to strain sensing, the interaction with oxygen molecules through adsorption and desorption processes by CNT and graphene under UV irradiation makes them suitable for achieving a stretchable photodetector. Previous studies found that oxygen molecules strongly adsorb on the surfaces and trap electrons when MWCNT/graphene is exposed to air, increasing their hole carrier concentration [21]. Upon exposure to UV light, the binding of oxygen molecules to MWCNT/graphene is disrupted by light-induced π-electron plasmons, resulting in the desorption of oxygen molecules from their surfaces and the return of captured electrons [21, 22].

In this study, we integrated 1D multi-walled CNT (MWCNT) and 2D graphene as sensing materials for strain sensors with high sensitivity and stretchability. They have high electrical conductivity and excellent mechanical properties [23], and the small difference in work function between MWCNTs and graphene enables charges to be transferred between them more efficiently [24]. We first studied the electromechanical performance of the MWCNT-based sensor with respect to the mass of MWCNTs coated on ~ 200 mm^2 of Ecoflex surface. The results demonstrated that the percolation networks of the sensor were gradually saturated when the sprayed MWCNT mass reached 0.18 mg. At this point, the sensor had a stretchable range of up to 814.17%. After adding 0.36 mg of graphene to 0.18 mg of MWCNTs (i.e., MWCNT to graphene mass ratio of 1:2), the easily detachable property of the graphene network under strain enabled the strain sensor to have a large GF of up to 12,144.7 in a strain range of 650–700%. The wide strain range of up to 710.5% is caused by the high aspect ratio of MWCNTs that bridge the randomly distributed graphene. The MWCNT/graphene hybrid sensor also exhibited stability over 600 loading–unloading cycles of 500% strain. Furthermore, because of the excellent sensitivity of MWCNT and graphene to oxygen molecules under UV irradiation and the small work function difference between them, the MWCNT/graphene-based strain sensor exhibited a photoresponse to UV light under 300% strain. The combination of MWCNT and graphene could be helpful in fabricating stretchable, multifunctional sensors.

Results and discussion

As described in Fig. 1a, the MWCNT/graphene dispersion obtained by 1 h of bath sonication was spray-coated onto the Ecoflex substrate, which was cut into a bone shape. A shadow mask was aligned on the Ecoflex substrate to define the coating region, resulting in the spray coating of MWCNT-graphene over an area of 5×40 mm^2. The photographs of the fabricated MWCNT-, graphene-, and MWCNT/graphene hybrid-based sensors are shown in Fig. 1a. In order to avoid excessive confinement of the sensing materials on the Ecoflex surface [7, 25, 26], the MWCNT and graphene are directly spray-coated on the sticky Ecoflex surface [27, 28] and tested without encapsulation. Scanning electron microscopy (SEM) images of graphene and MWCNT coated on a glass substrate are shown in Additional file 1: Fig. S1a and S1b. Based on the SEM images, statistical size distributions are characterized and results show that the size of graphene sheet is mostly distributed around 20 μm^2 (Additional file 1: Fig. S1c). In addition, the dominant length and diameter of MWCNT are mostly around 0.5–1 μm and 60–70 nm, respectively (Additional file 1: Fig. S1d and S1e). The spray-coated MWCNTs and graphene were randomly distributed on the Ecoflex substrate, as shown in the SEM images (Fig. 1b). This is caused by the formation of tiny dispersion droplets on the hydrophobic Ecoflex surfaces during spray coating of MWCNT/graphene dispersion [29, 30]. The randomly distributed droplets evaporate rapidly under a high temperature (90 °C) produced by a hot plate under the samples. Random MWCNT/graphene dispersed in the droplets remains on the Ecoflex surface.

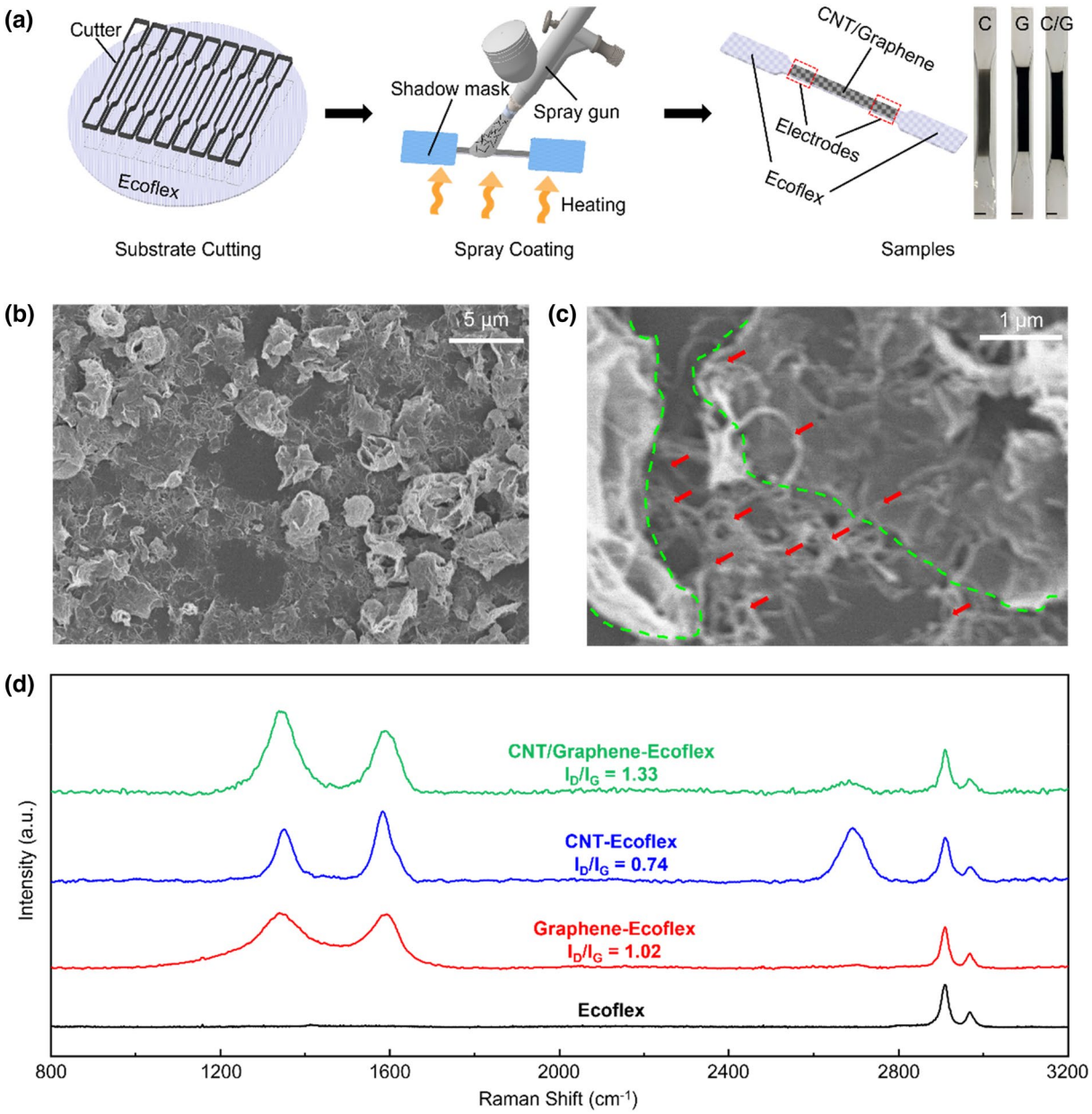

Fig. 1 **a** Schematic of the fabrication process of the MWCNT/graphene hybrid sensor. All scale bars in the photographs of the sensors are 5 mm. **b** SEM images of MWCNT/graphene hybrids. The MWCNT and graphene are randomly distributed on the Ecoflex substrate. **c** Partial enlargement of **b**. The green dotted line is the edge of graphene and the red arrows indicate the MWCNTs that bridge the graphenes. **d** Raman spectra of pristine Ecoflex, MWCNT-, graphene-, and MWCNT-graphene-coated Ecoflex.

This random distribution of the sensing layer makes the overall conductive path of the strain sensor easier to break, providing an opportunity to improve the GF of the sensor. An enlarged view of the SEM image (Fig. 1c) illustrates that a portion of MWCNTs (red arrows) are interleaved between graphenes (within green dashed lines) in the form of bridges. These MWCNTs contribute to maintaining sensor stretchability.

Raman spectra of pristine Ecoflex, MWCNT, graphene, and MWCNT/graphene hybrid-coated Ecoflex were obtained under excitation at 532 nm (Fig. 1d). Compared with the Raman spectrum of pristine Ecoflex (black line in Fig. 1d), the Raman spectra of graphene-, MWCNT-, and MWCNT/graphene-Ecoflex exhibit characteristic peaks for carbon-based materials (red, blue, and green lines in Fig. 1d) such as D-bands at 1339, 1351, and

1338 cm^{-1} from the disorder present in the sp^3 hybrid carbon system, G-bands at 1588, 1583, and 1589 cm^{-1} from the stretching of the C–C bonds in the graphite lattice, and 2D bands at 2703, 2693, and 2697 cm^{-1} [31]. Compared with MWCNT, the intensity of the 2D peak in the MWCNT/graphene hybrid decreases. We used the monolayer graphene produced by thermal exfoliation and hydrogen reduction methods. During this process, surface-abundant functional groups of graphite oxide increase the interlayer spacing from 0.34 to ~ 0.65–0.75 nm [32, 33]. The subsequent increase in temperature or pressure leads to escaping gases at the interlayer spacing, thus lifting off the graphene oxide. The exfoliated graphene oxides are then reduced by hydrogen to form monolayer graphene [34, 35]. Eventually, the surface of monolayer graphene prepared by a repeated oxidation–reduction process has a large number of defects and residual functional groups, which could result in a weak intensity of 2D peaks in the Raman spectrum of monolayer graphene [35–37]. The intensity ratio (I_D/I_G) between the D and G peaks, which provide information on interactions and structural defects in carbon-based materials, are 1.02, 0.74, and 1.33 for graphene, MWCNT, and MWCNT/graphene hybrid. The high I_D/I_G ratios of graphene and MWCNT/graphene hybrids compared with MWCNT also indicate the presence of a large number of defects in the graphene-containing samples.

The stretchable range and GF of the strain sensor can be modulated by adjusting the mass of MWCNTs and graphene and the ratio of MWCNTs and graphene. We investigated the sensing properties of the strain sensors composed of MWCNTs only with different spray-coated quantities to ensure high sensor stretchability. Given the intrinsic high aspect ratio of MWCNTs, the percolation networks of the sensing layer respond to tensile loads by sliding and fracture of connections between adjacent MWCNTs. As depicted in Fig. 2a, the stretchability of the sensor increases with the mass of the spray-coated MWCNTs in the given area (~ 200 mm^2). The stretchable range of the sensor increases sharply from 300 to 814.17% when the mass of the spray-coated MWCNTs increases from 0.12 to 0.18 mg. However, when the mass of MWCNTs increases by more than 0.18 mg, the increase rate of the stretchable range of the sensor slows down significantly and finally broke at 930% (MWCNT mass of 0.36 mg). This result indicates that the percolation networks of the sensor are gradually saturated after the mass of MWCNTs reaches 0.18 mg, caused by the increased number of conductive pathways in the sensor with increasing MWCNTs mass. However, the increased conductive pathways also cause a gradual decrease in the sensitivity, as depicted in Fig. 2a. For all cases, the relative resistance change of the sensor increases nonlinearly with an increase in the strain. The resistance change in the sensor under a small strain is caused primarily by the sliding between MWCNTs. As the strain increases, the conductive pathways between the sliding MWCNTs gradually break, causing a more significant resistance change.

We improved the GF of the sensor by incorporating 2D monolayer graphene into the 1D MWCNTs network. The 2D graphene with a relatively low aspect ratio makes the conductive pathways between the sensing materials more prone to strain fractures, resulting in high strain sensitivity of the sensor. A mass of 0.18 mg of MWCNTs, the amount where percolation networks and stretchability saturates, was chosen as the basis for incorporating graphene. The MWCNTs and graphene were mixed in mass ratios of 1:1.5, 1:2, and 1:3. As the mass of the incorporated graphene increases, the GF of the sensor gradually increases, while the stretchable range gradually decreases, as depicted in Fig. 2b. The improved GF could be caused by the formation of MWCNT bridges between graphenes (Fig. 1b, c). In the small strain range, the sliding between the sensing materials dominates the resistance change of the sensor, which produces a small resistance change in the sensor. However, graphene-graphene and graphene-MWCNTs networks can be easily fractured under a wide strain range, producing larger resistance changes. As shown in Additional file 1: Fig. S2, the sensing layer of the MWCNT-based sensor does not show obvious cracks even at a large strain of 550% due to the high aspect ratio and dense conductive network of MWCNTs (Additional file 1: Fig. S2a). On the other hand, as shown in Additional file 1: Fig. S2b and S2c, the cracks are formed under stretching in the graphene- and MWCNT/graphene-based sensors. Particularly, the graphene-based sensor shows a few discontinuities due to the formation of large cracks as indicated by green dotted lines in Additional file 1: Fig. S2b, which limit the stretchability of the sensor below 300%. The MWCNT/graphene-based sensor produces many smaller cracks than the graphene-based sensor due to the incorporation of MWCNTs with a high aspect ratio (Additional file 1: Fig. S2c), enabling high stretchability. In addition, the relative resistance change in the MWCNT/graphene hybrid sensor increased nonlinearly with increasing strain. The strain sensor fabricated with a mass ratio of 1:2 exhibits both a large GF (12,144.7, in a strain range of 650–700%) and a wide strain range (710.5%), as depicted in the yellow bar in Fig. 2c. This characteristic can be applicable for monitoring significant strain with high sensitivity.

The strain responses of the MWCNT-graphene hybrid sensor with a mass ratio of 1:2 were further investigated. As depicted in Fig. 3a, upon the loading–unloading from 0% to 10–600% of tensile strain, the sensor response was

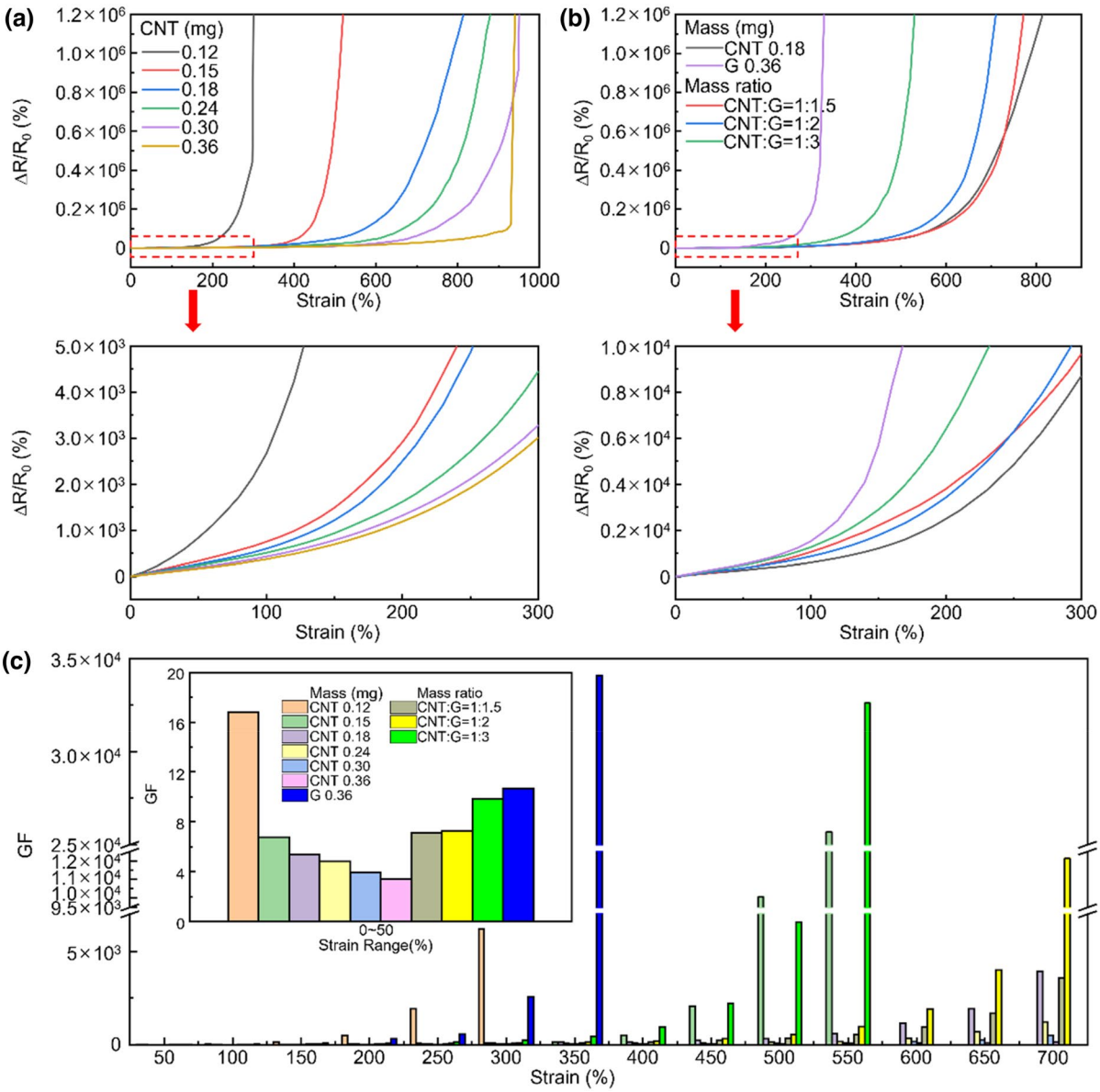

Fig. 2 Electromechanical performance of MWCNT/graphene hybrid sensor. **a** Strain sensing characteristic of the MWCNT-based sensor according to the mass of the coated MWCNTs (unit: mg). **b** Strain sensing characterization of MWCNT-, graphene-, and MWCNT/graphene hybrid-based sensors with different mass ratios. For both **a** and **b**, the partially enlarged views of the relative resistance change in the sensors at a strain range of 0–300% are depicted below them. Loading speed for all experiments is 2 mm/s. **c** GF of the MWCNT-, graphene-, and MWCNT/graphene hybrid-based sensors in a strain range of 0–700% for a 50% strain step. The strain sensor prepared by spray coating 0.36 mg graphene has the largest GF (~ 34,101.5), but the sensing range is limited to 330%. In contrast, the strain sensor composed of a hybrid of 1D MWCNT and 2D graphene with a mass ratio of 1:2 exhibits both a high GF of 12,144.7 (at a strain range of 650% ~ 700%) and a high sensing range of 710.5%

reversibly recovered to its initial state with some degree of hysteresis caused by the viscoelasticity of the Ecoflex substrate. These reversible strain responses indicate the high elasticity and stretchability of the sensor. The relative resistance change in the MWCNT/graphene hybrid sensor under cyclic strain in a strain range of 50–600% is depicted in Fig. 3b. The responses of the sensor under different strains remained almost unchanged during the 10 cycles of the loading–unloading process, indicating that the sensor has adequate repeatability. The reliability and durability of the strain sensor in practical applications are also important. The durability of the sensor was evaluated by periodic stretch-release cycling (500% strain). As depicted in Fig. 3c, the signal drift was ~ 5%

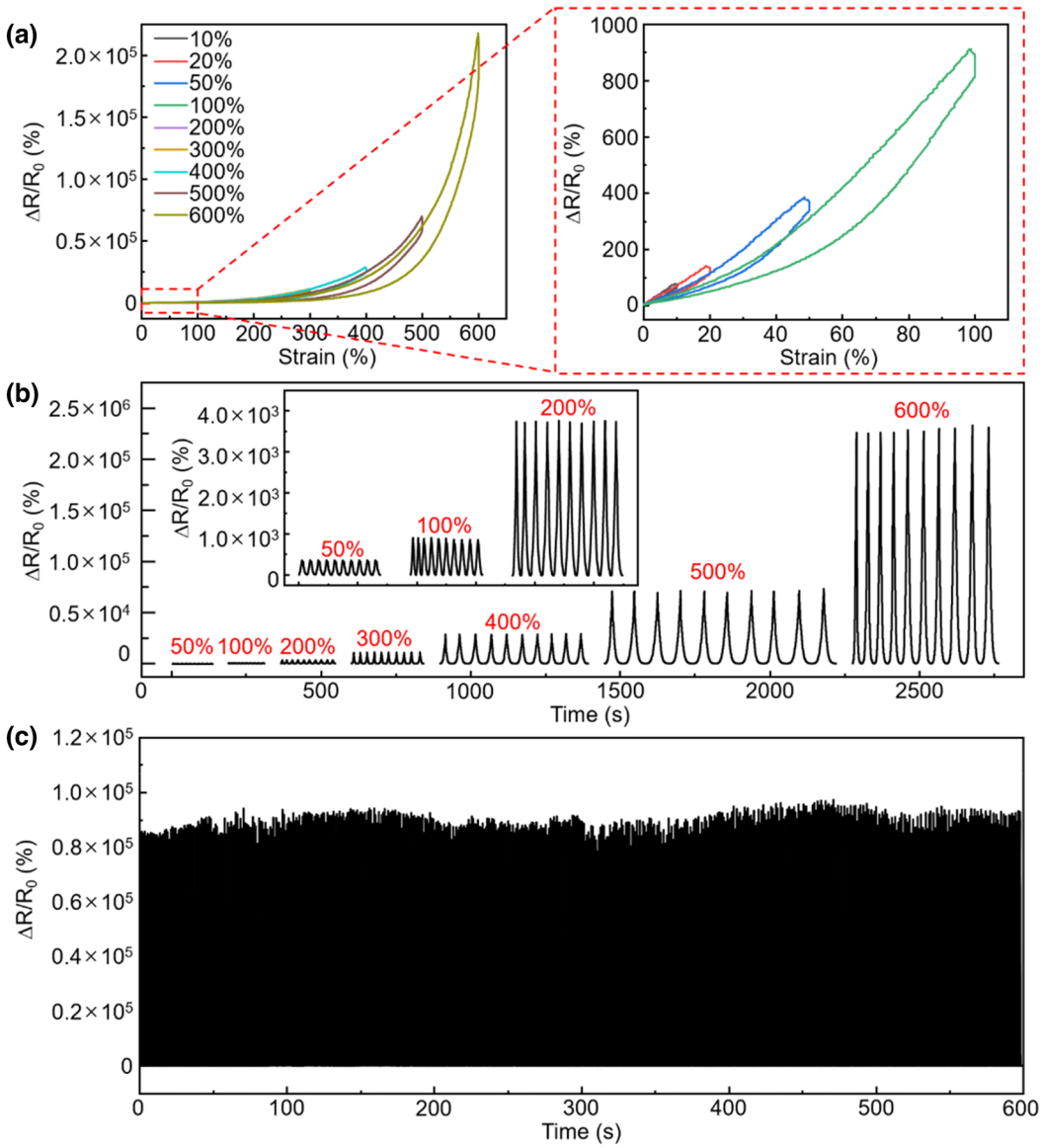

Fig. 3 **a** Hysteresis of MWCNT/graphene hybrid sensor (MWCNT: graphene = 1:2) strain from 10 to 600%. Partially enlarged view of **a** is in the right panel. **b** Strain responses of the sensor at the repeatably applied strains of 50, 100, 200, 300, 400, 500, and 600%. The inset is an enlarged view of the responses at 50, 100, and 200% strains. Loading speed for all tests was 2 mm/s. **c** Stability during 600 cycles under 500% strain

during 600 cycles. The signal drift is attributed to the instability of the conductive pathway under repeatedly applied large strain, which could be due to the peel-off of the sensing materials from the Ecoflex substrate [7, 38].

We demonstrated a stretchable photodetector by investigating the photoresponses of MWCNT-, graphene-, and MWCNT/graphene hybrid-based sensors to UV light with a wavelength of 365 nm in different stretched states. The distance between the sensor and the UV light source was fixed to 10 cm for all experiments. The sprayed quantities of MWCNT and graphene for homogeneous carbon nanomaterial-based sensors were 0.18 and 0.36 mg, while the MWCNT/graphene hybrid was spray-coated at a mass ratio of 1:2 (0.18:0.36 mg). As depicted in Fig. 4a, compared with MWCNT- and graphene-based sensors, the MWCNT/graphene hybrid sensors exhibit a larger response to UV light under all strains tested because more MWCNTs and graphene are involved in the response in the MWCNT/graphene hybrid sensor with the formation of abundant conductive pathways. Furthermore, the small difference in work function between MWCNT and graphene could attribute

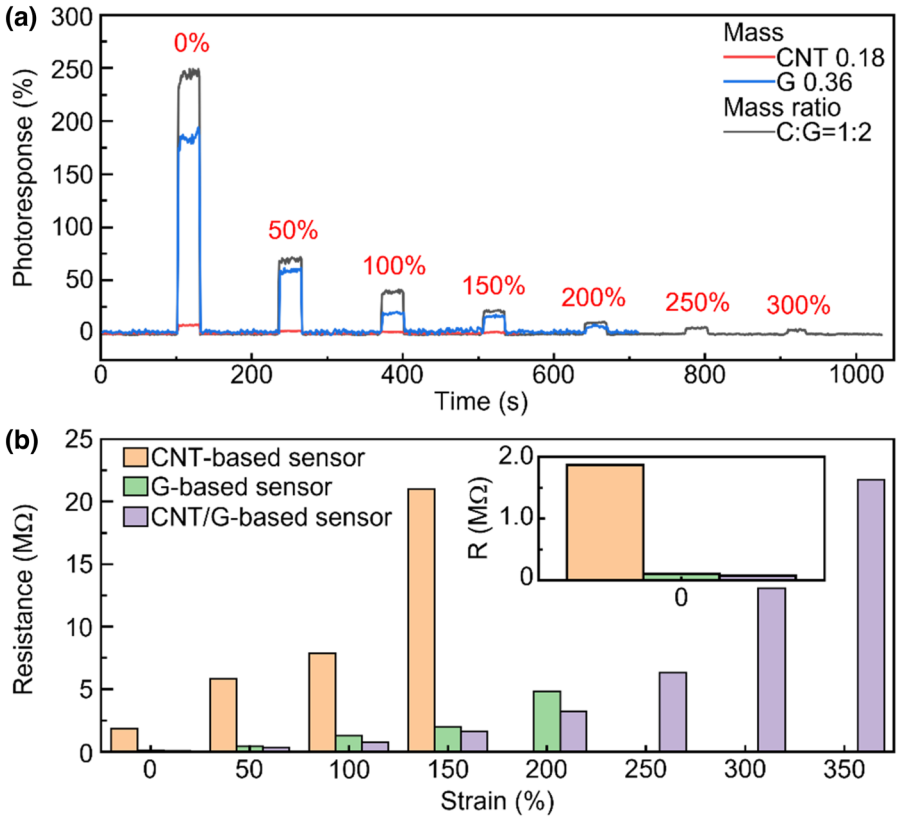

Fig. 4 **a** Photoresponses of MWCNT-, graphene-, and MWCNT/graphene hybrid-based sensors to UV light (365 nm) under different strains. The MWCNT/graphene hybrid sensor has the highest photoresponse compared with other sensors across the strain range tested. The MWCNT/graphene hybrid can measure photoresponses under high strains of over 250%. **b** The resistance of the MWCNT-, graphene-, and MWCNT/graphene hybrid-based sensors at different strains in the dark. Inset is an enlarged view of the sensor resistance at 0% strain

more efficient transfer of photogenerated charge carriers [21, 39, 40], resulting in a high photoresponse of 250% under 0% strain. The MWCNT- and graphene-based sensors no longer respond to UV light over strains exceeding 150% and 200%, although their stretchable range can reach 300% of strain. The MWCNT-based sensor exhibited the smallest response to UV light because of the high resistance of the sensor, which hinders the efficient transport of photogenerated carriers (Fig. 4b). The MWCNT/graphene hybrid sensor can respond to UV light under 300% strain. To calibrate the effect of temperature changes on the experimental results during UV sensing, we measured the temperature change of the sensors during seven on–off cycles of UV sensing by contacting a thermocouple on top of the sensing layer. As shown in Additional file 1: Fig. S3a, the temperature of the sensor surface increased from 24.7 to 36.57 °C under UV exposure, which can be due to heat transfer from the UV lamp. In addition, we separately measured the relative current change of the MWCNT-, graphene-, and MWCNT/graphene-based sensors in the temperature range of 23.75–40 °C (Additional file 1: Fig. S3b). Based on the measured data, the temperature response of the sensor was characterized (Additional file 1: Table S1), and it was compensated according to the measured temperature and temperature responses, which was reflected in Fig. 4a. The results imply that the mixture of CNT and graphene can not only improve the sensitivity of the strain sensor but also contribute to improve photoresponse even under stretched state.

Conclusion

We investigated the piezoresistive strain sensors by mixing 0.36 mg of graphene into 0.18 mg of MWCNT to achieve a high sensitivity and wide sensing range. The percolation network is formed by the MWCNTs that bridge the graphene flakes on the Ecoflex substrate. The hybrid of MWCNT and graphene produces a high GF (12,144.7 in the 650–700% strain range) while maintaining a stretchable range up to ~ 710.5%. The experimental results illustrate that the MWCNT/graphene-based sensor exhibits reversible responses up

to 600% tensile strain with high durability, as demonstrated by 600 cyclic loading–unloading of 500% strain. Furthermore, the UV sensing results demonstrate that the MWCNT/graphene-based sensor can respond to incident light in a strain range of 0–300%, and the response to UV light is as high as 250%. Our sensor fabricated by mixing MWCNTs and graphene in a 1:2 mass ratio exhibits high sensitivity and stretchability. It could be a building block for achieving multifunctional wearable devices that require mechanical deformability.

Abbreviations

1D: One-dimensional; 2D: Two-dimensional; CNT: Carbon nanotube; GF: Gauge factor; PDMS: Polydimethylsiloxane; UV: Ultraviolet; MWCNT: Multi-walled carbon nanotube; G: Graphene.

Supplementary Information

The online version contains supplementary material available at https://doi.org/10.1186/s40486-022-00160-9.

Additional file 1: Figure S1. SEM image of **a** graphene and **b** MWCNT coated on a glass substrate. **c**–**e** Column charts of size statistics of graphene (c), length and diameter statistics of MWCNT (d,e). The statistical results show that the size of graphene sheet is mostly distributed around 20 μm^2. In addition, the dominant length and diameter of MWCNT are mostly around 0.5-1 μm and 60-70 nm, respectively. **Figure S2.** Photographs and optical microscope images of **a** MWCNT-, **b** graphene-, and **c** MWCNT/graphene hybrid-based sensor at 0% and 550% strain. No obvious cracks are observed in the MWCNT-based sensor under 550% strain, but significant cracks are formed once the graphene is added to the sensing layer. This can be due to the easy separation of graphene under large stretching. It is noted that the size of cracks is smaller in the MWCNT/graphene-based sensor than in the graphene-based sensor, which might be due to the high aspect ratio of MWCNTs that bridge the graphene flakes. **Figure S3. a** Temperature change of the sensor surface for seven cycles of UV sensing. The temperature of the sensor surface increased from 24.7°C to 36.57°C owing to heat transfer from the UV lamp. **b** Relative current change of the MWCNT-, graphene-, and MWCNT/graphene hybrid-based sensors during the temperature increased from 23.75°C to 40°C. **Table S1.** Relative current change of MWCNT-, graphene-, and MWCNT/graphene hybrid-based sensors caused by the temperature changes during each UV on-off cycle shown in Fig. 4a.

Acknowledgements

Not applicable.

Author contributions

All authors contributed to writing and editing the manuscript and approved the final manuscript.

Funding

This research was supported by the Basic Science Research Program through the National Research Foundation of Korea (NRF), funded by the Ministry of Science, ICT, and Future Planning (2022R1A2C4001577).

Availability of data and materials

Not applicable.

Declarations

Competing interests

The authors declare that they have no competing interests.

Received: 14 September 2022 Accepted: 3 November 2022
Published online: 12 November 2022

References

1. Ma J, Wang P, Chen H, Bao S, Chen W, Lu H (2019) Highly sensitive and large-range strain sensor with a self-compensated two-order structure for human motion detection. ACS Appl Mater Interfaces 11:8527–8536
2. Kang S-J, Pak JJ (2017) A review: flexible, stretchable multifunctional sensors and actuators for heart arrhythmia therapy. Micro Nano Syst Lett 5:22
3. He Y, Wu D, Zhou M, Zheng Y, Wang T, Lu C, Zhang L, Liu H, Liu C (2021) Wearable strain sensors based on a porous polydimethylsiloxane hybrid with carbon nanotubes and graphene. ACS Appl Mater Interfaces 13:15572–15583
4. Yamada T, Hayamizu Y, Yamamoto Y, Yomogida Y, Izadi-Najafabadi A, Futaba DN, Hata K (2011) A stretchable carbon nanotube strain sensor for human-motion detection. Nat Nanotechnol 6:296–301
5. Wang L, Choi W, Yoo K, Nam K, Ko TJ, Choi J (2020) Stretchable carbon nanotube dilatometer for in situ swelling detection of lithium-ion batteries. ACS Appl Energy Mater 3:3637–3644
6. Wu JM, Chen C-Y, Zhang Y, Chen K-H, Yang Y, Hu Y, He J-H, Wang ZL (2012) Ultrahigh sensitive piezotronic strain sensors based on a $ZnSnO_3$ nanowire/microwire. ACS Nano 6:4369–4374
7. Amjadi M, Pichitpajongkit A, Lee S, Ryu S, Park I (2014) Highly stretchable and sensitive strain sensor based on silver nanowire-elastomer nanocomposite. ACS Nano 8:5154–5163
8. De Oliveir JG, Muhammad T, Kim S (2020) A silver nanowire-based flexible pressure sensor to measure the non-nutritive sucking power of neonates. Micro Nano Syst Lett 8:18
9. Boland CS, Khan U, Backes C, O'Neill A, Mccauley J, Duane S, Shanker R, Liu Y, Jurewicz I, Dalton AB, Coleman JN (2014) Sensitive, high-strain, high-rate bodily motion sensors based on graphene–rubber composites. ACS Nano 8:8819–8830
10. Jung Y, Jung K, Park B, Choi J, Kim D, Park J, Ko J, Cho H (2019) Wearable piezoresistive strain sensor based on graphene-coated three-dimensional micro-porous PDMS sponge. Micro Nano Syst Lett 7:20
11. Yang H, Xiao X, Li Z, Li K, Cheng N, Li S, Low JH, Jing L, Fu X, Achavanan-thadith S, Low F, Wang Q, Yeh P-L, Ren H, Ho JS, Yeow C-H, Chen P-Y (2020) Wireless $Ti_3C_2T_x$ MXene strain sensor with ultrahigh sensitivity and designated working windows for soft exoskeletons. ACS Nano 14:11860–11875
12. Chao M, Wang Y, Ma D, Wu X, Zhang W, Zhang L, Wan P (2020) Wearable MXene nanocomposites-based strain sensor with tile-like stacked hierarchical microstructure for broad-range ultrasensitive sensing. Nano Energy 78:105187
13. Pan S, Pei Z, Jing Z, Song J, Zhang W, Zhang Q, Sang S (2020) A highly stretchable strain sensor based on CNT/graphene/fullerene-SEBS. RSC Adv 10:11225–11232
14. Chen S, Wei Y, Yuan X, Lin Y, Liu L (2016) A highly stretchable strain sensor based on a graphene/silver nanoparticle synergic conductive network and a sandwich structure. J Mater Chem C 4:4304–4311
15. Cai Y, Shen J, Ge G, Zhang Y, Jin W, Huang W, Shao J, Yang J, Dong X (2018) Stretchable $Ti_3C_2T_x$ MXene/carbon nanotube composite based strain sensor with ultrahigh sensitivity and tunable sensing range. ACS Nano 12:56–62
16. Qiu D, Chu Y, Zeng H, Xu H, Dan G (2019) Stretchable MoS_2 electromechanical sensors with ultrahigh sensitivity and large detection range for skin-on monitoring. ACS Appl Mater Interfaces 11:37035–37042
17. Wang C, Xia K, Wang H, Liang X, Yin Z, Zhang Y (2019) Advanced carbon for flexible and wearable electronics. Adv Mater 31:1801072
18. Pyo S, Eun Y, Sim J, Kim K, Choi J (2022) Carbon nanotube-graphene hybrids for soft electronics, sensors, and actuators. Micro Nano Syst Lett 10:9
19. Amjadi M, Yoon YJ, Park I (2015) Ultra-stretchable and skin-mountable strain sensors using carbon nanotubes-ecoflex nanocomposites. Nanotechnology 26:375501
20. Li X, Yang T, Yang Y, Zhu J, Li L, Alam FE, Li X, Wang K, Cheng H, Lin C-T, Fang Y, Zhu H (2016) Large-area ultrathin graphene films by single-step marangoni self-assembly for high sensitive strain sensing application. Adv Funct Mater 26:1322–1329

21. Pyo S, Choi J, Kim J (2019) A fully transparent, flexible, sensitive, and visible-blind ultraviolet sensor based on carbon nanotube-graphene hybrid. Adv Electron Mater 5:1–8
22. Zhang Y, Deng T, Li S, Sun J, Yin W, Fang Y, Liu Z (2020) Highly sensitive ultraviolet photodetectors based on single wall carbon nanotube-graphene hybrid films. Appl Surf Sci 512:145651
23. Park S, Vosguerichian M, Bao Z (2013) A review of fabrication and applications of carbon nanotube film-based flexible electronics. Nanoscale 5:1727–1752
24. Jang S, Jang H, Lee Y, Suh D, Baik S, Hong HB, Ahn J-H (2010) Flexible, transparent single-walled carbon nanotube transistors with graphene electrodes. Nanotechnology 21:425201
25. Liu Y, Sheng Q, Muftu S, Khademhosseini A, Wang ML, Dokmeci MR (2013) A stretchable and transparent SWNT strain sensor encapsulated in thin PDMS films. In: Proceedings of the 2013 Transducers & Eurosensors XXVII: The 17th international conference on solid-state sensors, actuators and microsystems (TRANSDUCERS & EUROSENSORS XXVII), Barcelona, Spain, pp 1091–1094
26. Liu M-Y, Hang C-Z, Wu X-Y, Zhu L-Y, Wen X-H, Wang Y, Zhao X-F, Lu H-L (2022) Investigation of stretchable strain sensor based on CNT/AgNW applied in smart wearable devices. Nanotechnology 33:255501
27. Darby DR, Cai Z, Mason CR, Pham JT (2022) Modulus and adhesion of Sylgard 184, solaris, and Ecoflex 00-30 silicone elastomers with varied mixing ratios. J Appl Polym Sci 139:e52412
28. Yu Y, Sanchez D, Lu N (2015) Work of adhesion/separation between soft elastomers of different mixing ratios. J Mater Res 30:2702–2712
29. Lu Z, Song J, Pan K, Meng J, Xin Z, Liu Y, Zhao Z, Gong RH, Li J (2019) Ecoflex sponge with ultrahigh oil absorption capacity. ACS Appl Mater Interfaces 11:20037–20044
30. Alcântara CCJ, Landers FC, Kim S, De Marco C, Ahmed D, Nelson BJ, Pané S (2020) Mechanically interlocked 3D multi-material micromachines. Nat Commun 11:5957
31. Bagotia N, Choudhary V, Sharma DK (2019) Synergistic effect of graphene/multiwalled carbon nanotube hybrid fillers on mechanical, electrical and EMI shielding properties of polycarbonate/ethylene methyl acrylate nanocomposites. Compos Part B Eng 159:378–388
32. Mcallister MJ, Li J-L, Adamson DH, Schniepp HC, Abdala AA, Liu J, Herrera-Alonso M, Milius DL, Car R, Prud'homme RK, Aksay IA (2007) Single sheet functionalized graphene by oxidation and thermal expansion of graphite. Society 19:4396–4404
33. Schniepp HC, Li J-L, McAllister MJ, Sai H, Herrera-Alonso M, Adamson DH, Prud'homme RK, Car R, Seville DA, Aksay IA (2006) Functionalized single graphene sheets derived from splitting graphite oxide. J Phys Chem B 110:8535–8539
34. Zhang C, Lv W, Xie X, Tang D, Liu C, Yang Q-H (2013) Towards low temperature thermal exfoliation of graphite oxide for graphene production. Carbon 62:11–24
35. Stankovich S, Dikin DA, Piner RD, Kohlhaas KA, Kleinhammes A, Jia Y, Wu Y, Nguyen SBT, Ruoff RS (2007) Synthesis of graphene-based nanosheets via chemical reduction of exfoliated graphite oxide. Carbon 45:1558–1565
36. Kaniyoor A, Ramaprabhu S (2012) A Raman spectroscopic investigation of graphite oxide derived graphene. AIP Adv 2:032183
37. Botas C, Álvarez P, Blanco C, Santamaría R, Granda M, Gutiérrez MD, Rodríguez-Reinoso F, Menéndez R (2013) Critical temperatures in the synthesis of graphene-like materials by thermal exfoliation-reduction of graphite oxide. Carbon 52:476–485
38. Fan Q, Qin Z, Gao S, Wu Y, Pionteck J, Mäder E, Zhu M (2012) The use of a carbon nanotube layer on a polyurethane multifilament substrate for monitoring strains as large as 400%. Carbon 50:4085–4092
39. Shiraishi M, Ata M (2001) Work function of carbon nanotubes. Carbon 39:1913–1917
40. Yu Y-J, Zhao Y, Ryu S, Brus LE, Kim KS, Kim P (2009) Tuning the graphene work function by electric field effect. Nano Lett 9:3430–3434

Publisher's Note

Springer Nature remains neutral with regard to jurisdictional claims in published maps and institutional affiliations.

Submit your manuscript to a SpringerOpen journal and benefit from:

- ► Convenient online submission
- ► Rigorous peer review
- ► Open access: articles freely available online
- ► High visibility within the field
- ► Retaining the copyright to your article

Submit your next manuscript at ► springeropen.com